

Skewness-Robust Causal Discovery in Location-Scale Noise Models

Daniel Klippert^{1,2}, Alexander Marx^{1,2}

¹Department of Statistics, TU Dortmund University

²Research Center Trustworthy Data Science and Security, University Alliance Ruhr
{daniel.klippert,alexander.marx}@tu-dortmund.de

Abstract

To distinguish Markov equivalent graphs in causal discovery, it is necessary to restrict the structural causal model. Crucially, we need to be able to distinguish cause X from effect Y in bivariate models, that is, distinguish the two graphs $X \rightarrow Y$ and $Y \rightarrow X$. Location-scale noise models (LSNMs), in which the effect Y is modeled based on the cause X as $Y = f(X) + g(X)N$, form a flexible class of models that is general and identifiable in most cases. Estimating these models for arbitrary noise terms N , however, is challenging. Therefore, practical estimators are typically restricted to symmetric distributions, such as the normal distribution. As we showcase in this paper, when N is a skewed random variable, which is likely in real-world domains, the reliability of these approaches decreases. To approach this limitation, we propose SKEWD, a likelihood-based algorithm for bivariate causal discovery under LSNMs with skewed noise distributions. SKEWD extends the usual normal-distribution framework to the skew-normal setting, enabling reliable inference under symmetric and skewed noise. For parameter estimation, we employ a combination of a heuristic search and an expectation conditional maximization algorithm. We evaluate SKEWD on novel synthetically generated datasets with skewed noise as well as established benchmark datasets. Throughout our experiments, SKEWD exhibits a strong performance and, in comparison to prior work, remains robust under high skewness.

1 Introduction

Causal discovery describes the process of learning cause-effect relationships from observational data and is of strong interest across most scientific fields, including Earth sciences (Runge et al. 2019), neuroscience (Ramsey et al. 2010) and manufacturing (Vuković and Thalmann 2022). We study causal discovery from independently and identically distributed (iid) data, concentrating on approaches that impose restrictions on the structural causal model (SCM). Compared to classical constraint-based or score-based methods (Spirtes, Glymour, and Scheines 2000; Chickering 2002), these approaches yield identification results that differentiate Markov equivalent DAGs. A key aspect is the identification of edges between pairs of variables, which cannot be achieved by conditional independence testing.

In the bivariate case, where we are provided with data from two random variables X and Y , causal discovery is

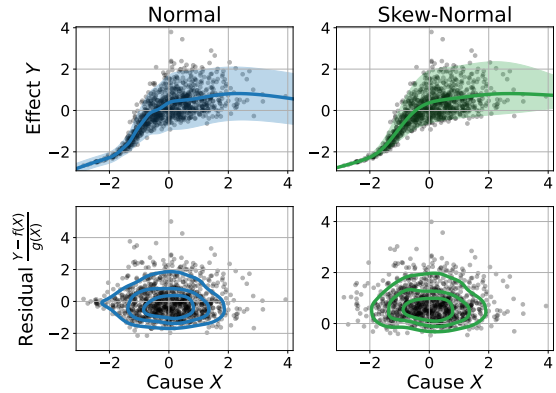


Figure 1: Comparison of LSNM mean fits and confidence intervals based on the normal distribution via LOCI (left) and skew-normal distribution via SKEWD (right) for pair 6 from the novel LSs(1.750) dataset. The estimated residuals in the normal-model display a dependence with cause X , indicated by the pointy outer contour level of the kernel density estimate for small X , leading to a wrong inference. SKEWD overcomes this limitation and infers the correct direction.

concerned with the question whether $X \rightarrow Y$ (X causes Y) or $X \leftarrow Y$ (Y causes X). In general, an SCM consistent with $X \rightarrow Y$ entails the functional relationship $Y = f(X, N)$, where N is a noise variable that is independent of X . Without further assumptions on the SCM, the causal direction is not identifiable based on the joint distribution $P_{X,Y}$ (Peters, Janzing, and Schölkopf 2017, Ch. 4). Approaches that restrict the functional relationship to an identifiable functional model class overcome this issue. Simply put, the imposed assumptions break the symmetry of the joint distribution $P_{X,Y}$ under the two directions, such that only the true causal model can exhibit independent noise. Well-known approaches include linear non-Gaussian additive noise models (LiNGAM) (Shimizu et al. 2006), nonlinear additive noise models (nonlinear ANMs) (Hoyer et al. 2008), post-nonlinear (PNL) causal models (Zhang and Hyvärinen 2009), and location-scale noise models (LSNMs) (Immer et al. 2023).

In this paper, we focus on the class of LSNMs, for which the functional relationship between cause X and effect Y

is described by $Y = f(X) + g(X)N$, where g is a strictly positive function. LSNMs generalize the class of ANMs and have been shown to be identifiable except for pathological cases (Strobl and Lasko 2023; Immer et al. 2023). Despite the generality of the identification result, prior work predominantly modeled symmetric noise distributions (Immer et al. 2023; Strobl and Lasko 2023; Lin et al. 2024; Tran et al. 2024). This assumption is, however, often violated in real-world data, e.g., Genton (2004) provides numerous data examples exhibiting skewed distributions, including coastal flooding, spatial rainfall prediction and stochastic frontier analysis. In Fig. 1, we illustrate the problem that skewed noise distributions pose to these approaches. Here, we apply LOCI (Immer et al. 2023), which assumes Gaussian noise terms and follows a RESIT-type approach (Peters et al. 2014) to a skewed LSNM. Such approaches, aim to extract the noise term as $\hat{N} = (Y - \hat{f}(X))(\hat{g}(X))^{-1}$ and subsequently test for independence with the hypothetical cause X . Independence would confirm the model assumptions, however, we see that the skewness induces a misspecification in the learned functions, and consequently, independence is rejected. As demonstrated in our experiments, this problem persists when resorting to likelihood-based approaches, which suffer from the same misspecification issue. This observation is in line with prior work that highlighted the pitfalls of Gaussian likelihood scoring in causal discovery for linear ANMs (Reisach, Seiler, and Weichwald 2021) and LSNMs (Schultheiss and Bühlmann 2023).

By explicitly modeling the skewness, we stay within the identifiable model class of LSNMs, while covering a strictly larger class of noise distributions. In particular, our new method, SKEWD, models the noise distribution as skew-normal, which includes the normal distribution as a special case. In the example provided in Fig. 1, we can see that SKEWD effectively recovers the independent noise variable, thus inferring the correct causal direction. Concretely, our main contributions can be summarized as follows. In Sec. 2, we introduce the skew-normal location-scale noise model and propose a maximum likelihood estimation procedure. In Sec. 3, we detail our parameter estimation method, which refines the estimate of an initial heuristic optimization via an expectation conditional maximization algorithm. We discuss cause-effect inference in Sec. 4, and propose SKEWD as a practical approach based on residual independence testing or likelihood scoring. Further, we empirically compare SKEWD to state-of-the-art (SOTA) algorithms on established and novel benchmarks with varying skewness levels in Sec. 6. We find that SKEWD stands out as the most reliable approach for LSNMs under high skewness while performing on par with SOTA in other settings.¹

2 Modeling Skewness in LSNMs

In this section, we formally introduce the location-scale noise model and define the notion of skewness. We then

¹To ensure reproducibility, the implementation of our method and experimental runs are publicly available under <https://github.com/causality-lab/skewd>.

characterize the skew-normal distribution and describe the specific skew-normal LSNM used within our framework.

Definition 1 (Location-Scale Noise Models) Let X, Y, N_Y define continuous random variables and assume that X, N_Y are independent. Further, let \mathcal{X} denote the support of X . Then, the joint distribution $P_{X,Y}$ admits a location-scale noise model $X \rightarrow Y$ with cause X , effect Y and noise N_Y , if there exist functions $f : \mathcal{X} \rightarrow \mathbb{R}, g : \mathcal{X} \rightarrow \mathbb{R}_+$, such that

$$Y = f(X) + g(X)N_Y. \quad (1)$$

Definition 2 (Skewness) The skewness of a univariate random variable X with mean $\mathbb{E}[X] = \mu$ and variance $\mathbb{E}[(X - \mu)^2] = \sigma^2$ corresponds to the third centralized moment and is given by

$$\gamma_1 = \mathbb{E} \left[\left(\frac{X - \mu}{\sigma} \right)^3 \right].$$

A random variable is said to be skewed or asymmetric if $\gamma_1 \neq 0$. If $\gamma_1 > 0$, the random variable is right-skewed and if $\gamma_1 < 0$, it is left-skewed. The frequent assumption of normally distributed errors in statistical models limits their applicability due to the symmetry of the normal distribution. To ensure reliable cause-effect inference in settings that may include skewed noise, we propose to model the noise N_Y in Eq. (1) via the skew-normal distribution (Azzalini 1985).

Definition 3 (Skew-Normal Distribution) The random variable X follows a univariate skew-normal distribution with parameters $\xi \in \mathbb{R}$ (location), $\omega > 0$ (scale), and $\lambda \in \mathbb{R}$ (shape), $X \sim \text{SN}(\xi, \omega, \lambda)$, if its probability density function (pdf) is given by

$$p(x) = \frac{2}{\omega} \phi \left(\frac{x - \xi}{\omega} \right) \Phi \left(\lambda \frac{x - \xi}{\omega} \right), \quad x \in \mathbb{R}, \quad (2)$$

where ϕ and Φ correspond to the pdf and cumulative distribution function (cdf) of the standard normal distribution, respectively. The skewness of X is then calculated as

$$\gamma_1 = \frac{4 - \pi}{2} \frac{b^3 \delta^3}{(1 - b^2 \delta^2)^{3/2}},$$

where $b = \sqrt{2/\pi}$ and $\delta = \lambda/\sqrt{(1 + \lambda^2)}$. It follows that the skew-normal distribution is right-skewed if $\lambda > 0$ and left-skewed if $\lambda < 0$. The skewness of the skew-normal distribution is bounded by the interval $(-\gamma_1^{\max}, \gamma_1^{\max})$, where $\gamma_1^{\max} \approx 0.9953$ (Azzalini 2013). The skew-normal distribution $\text{SN}(\xi, \omega, \lambda)$ generalizes the normal distribution, since it reduces to a regular normal distribution with mean ξ and variance ω^2 if $\lambda = 0$. This ensures compatibility with the standard assumption of normally distributed symmetric noise making it a more natural choice than alternative asymmetric distributions like the asymmetric Laplace (Kozubowski and Podgorski 2000). We provide further details on the skew-normal distribution in Appendix A.

Skew-Normal LSNM The goal of this work is to distinguish between LSNMs $X \rightarrow Y$ and $Y \rightarrow X$ based on independent and identically distributed (iid) samples

$(x_1, y_1), \dots, (x_n, y_n)$, where the noise distribution may exhibit skewness. Within our framework, we assume that $N_Y \sim \text{SN}(0, 1, \lambda)$ in the LSM in Eq. (1). By the density transformation formula it follows that the conditional distribution of the effect given the cause is then skew-normally distributed with $Y|X = x \sim \text{SN}(f(x), g(x), \lambda)$. To allow for flexible functions f and g , we model these functions using natural cubic B-splines which may differ in the number of knots (Eilers and Marx 1996). Given the observed cause $x_i, i = 1, \dots, n$, we assume the cause-effect model

$$Y_i = f(x_i) + g(x_i)N_{Y_i} = \mathbf{n}_i^\top \boldsymbol{\psi} + \exp(0.5\mathbf{z}_i^\top \boldsymbol{\rho}) N_{Y_i}, \quad (3)$$

where $\mathbf{n}_i^\top \in \mathbb{R}^{1 \times q}$, $\mathbf{z}_i^\top \in \mathbb{R}^{1 \times p}$ correspond to the i -th row of the B-splines matrices $\mathbf{N} \in \mathbb{R}^{n \times q}$ and $\mathbf{Z} \in \mathbb{R}^{n \times p}$. The corresponding unknown coefficient vectors are denoted by $\boldsymbol{\psi} \in \mathbb{R}^q$, and $\boldsymbol{\rho} \in \mathbb{R}^p$. Similar to the approach of Ferreira, Borelli Zeller, and de Oliveira Garcia (2023), we apply the exponential function to ensure positivity of the estimated scale parameter. Performing cause-effect inference via likelihood scoring or independence testing (see Sec. 4) requires estimating the skew-normal LSMs $X \rightarrow Y$ and $Y \rightarrow X$, which we discuss in the next section.

3 Parameter Estimation

In order to estimate the skew-normal LSM $X \rightarrow Y$, we employ a maximum likelihood approach. In the following, we define the (penalized) log-likelihood and discuss our estimation approach, which includes an expectation conditional maximization algorithm described at the end of this section.

Model Log-Likelihood From Eq. (3) it follows that the observed log-likelihood of the effect $\mathbf{y} = (y_1, \dots, y_n)^\top$ given the cause $\mathbf{x} = (x_1, \dots, x_n)^\top$ with respect to the parameters $\boldsymbol{\theta} = (\boldsymbol{\psi}^\top, \boldsymbol{\rho}^\top, \lambda)^\top$ is given by

$$\begin{aligned} \ell(\boldsymbol{\theta}) = & \frac{n}{2} \log\left(\frac{2}{\pi}\right) - \frac{1}{2} \sum_{i=1}^n \mathbf{z}_i^\top \boldsymbol{\rho} - \frac{1}{2} \sum_{i=1}^n \frac{(y_i - \mathbf{n}_i^\top \boldsymbol{\psi})^2}{\exp(\mathbf{z}_i^\top \boldsymbol{\rho})} \\ & + \sum_{i=1}^n \log\left(\Phi\left(\lambda \frac{y_i - \mathbf{n}_i^\top \boldsymbol{\psi}}{\exp(0.5\mathbf{z}_i^\top \boldsymbol{\rho})}\right)\right). \end{aligned}$$

Penalized Log-Likelihood To prevent an overfitting behavior, we adopt a penalized log-likelihood approach that imposes roughness penalties based on second-order differences of the spline coefficients (Eilers and Marx 1996). Let

$$\mathbf{D}_r = \begin{bmatrix} 1 & -2 & 1 & 0 & \dots & 0 \\ 0 & 1 & -2 & 1 & \dots & 0 \\ \vdots & \ddots & \ddots & \ddots & \ddots & \vdots \\ 0 & \dots & 0 & 1 & -2 & 1 \end{bmatrix} \in \mathbb{R}^{(r-2) \times r}$$

define the second-order difference matrix with respect to dimensionality r . Then, the penalty matrices for $\boldsymbol{\psi}$ and $\boldsymbol{\rho}$ are given by $\mathbf{K} = \mathbf{D}_q^\top \mathbf{D}_q$ and $\mathbf{M} = \mathbf{D}_p^\top \mathbf{D}_p$. The explicit second-order difference penalty on $\boldsymbol{\psi}$ is given by

$$\boldsymbol{\psi}^\top \mathbf{K} \boldsymbol{\psi} = \sum_{j=3}^q (\psi_j - 2\psi_{j-1} + \psi_{j-2})^2$$

Algorithm 1: Estimate model parameters $\boldsymbol{\theta}$

- 1: Perform Bayesian optimization to find optimal α, κ
 - 2: Find $\hat{\boldsymbol{\theta}}_h = \text{argmax}_{\boldsymbol{\theta}} \ell_p(\boldsymbol{\theta}, \alpha, \kappa)$ via CMA-ES given α, κ
 - 3: Submit $\hat{\boldsymbol{\theta}}_h$ as initial value to ECM algorithm yielding final parameter estimate $\hat{\boldsymbol{\theta}}$
-

and analogously for $\boldsymbol{\rho}$ using \mathbf{M} . The resulting penalized log-likelihood is given by

$$\ell_p(\boldsymbol{\theta}, \alpha, \kappa) = \ell(\boldsymbol{\theta}) - \frac{\alpha}{2} \boldsymbol{\psi}^\top \mathbf{K} \boldsymbol{\psi} - \frac{\kappa}{2} \boldsymbol{\rho}^\top \mathbf{M} \boldsymbol{\rho}, \quad (4)$$

where the parameters $\alpha, \kappa > 0$ control the regularization strength. In our causal discovery method, we estimate the model parameters of the LSM in Eq. (3) by maximizing the penalized log-likelihood from Eq. (4).

Challenges in Optimization Maximizing the penalized log-likelihood defined in Eq. (4) involves two challenges. First, the hyperparameters α and κ must be selected to balance model fit and regularization. Secondly, given values of α and κ , a reliable maximization approach for this non-convex optimization problem is required, however, this is challenging for the skew-normal model, as further discussed in Sec. 5. We base our optimization approach on an expectation conditional maximization (ECM) algorithm by Ferreira, Borelli Zeller, and de Oliveira Garcia (2023). An advantage of expectation maximization (EM) type algorithms is that they increase or maintain the likelihood with every update (Dempster, Laird, and Rubin 1977; Meng and Rubin 1993), which also carries over when the penalized likelihood is maximized (Green 1990). However, they can exhibit slow convergence and are susceptible to converging to local optima (Karlis and Xekalaki 2003). A common countermeasure against local optima is to run the algorithm from multiple starting points and select the best result. However, since we consider a $(p + q + 1)$ -dimensional parameter space, this strategy may require numerous iterations making it computationally intensive.

Optimization Approach The main steps of our estimation approach are summarized in Algorithm 1. Instead of directly using an ECM algorithm, assuming for now we have fixed values for α and κ , we heuristically optimize the penalized likelihood using the covariance matrix adaptation evolution strategy (CMA-ES). The CMA-ES is an evolutionary optimization algorithm for non-linear, non-convex functions (Hansen and Ostermeier 2001; Hansen 2023). Since it is stochastic, we use multiple starting values for $\boldsymbol{\theta}$ and submit the best result to an ECM algorithm to refine the obtained heuristic solution (lines 2–3). In Appendix B, we show how the ECM algorithm improves upon the performance achieved by the initial heuristic solution in the causal discovery task on our synthetic data, demonstrating the necessity of refinement. Since the described approach requires fixed penalty parameters, we precede it with a Bayesian optimization step (line 1) to find adequate values for α and κ .

Bayesian Optimization To tune the penalty parameters, we employ a cross-validated model selection procedure based on Bayesian optimization (Frazier 2018). We generate initial candidate values using Latin Hypercube Sampling on the log-scale with $(\log(\alpha), \log(\kappa))^T \in [-4, 4]^2$. For each candidate pair, we perform a k -fold cross-validation. We maximize the penalized log-likelihood on the $k - 1$ training folds and evaluate the unpenalized log-likelihood on the held-out fold, since the goal is to identify penalty parameters that improve the generalization of the actual likelihood function. The average over the k unpenalized held-out likelihoods is the quantity being optimized through the Bayesian optimization, where the penalty parameters with the highest log-likelihood will be selected. While other optimizers could be employed in this heuristic framework, we use the CMA-ES in its implementation by Nomura and Shibata (2024) due to its robustness w.r.t. complex search landscapes with multiple local optima and sharp ridges. We refer to Appendix B for more details on implementation and hyperparameter settings used in our experiments (Sec. 6).

Expectation Conditional Maximization (ECM) ECM algorithms (Meng and Rubin 1993) iteratively derive maximum likelihood estimates within latent variable models by alternating between an expectation step (E-step) and a sequence of conditional maximization steps (CM-steps). In each iteration, the likelihood is increased (or maintained) by optimizing a lower bound, known as the Q -function which is computed in the E-step. It is the expected value of the complete data log-likelihood over the conditional distribution of the latent variables given the observed data and current parameter estimates. In the CM-steps, the parameter vector θ is updated by sequentially maximizing the Q -function with respect to subsets of the parameters while keeping the remaining parameter fixed.

In the following, we outline the ECM algorithm employed to refine the heuristic parameter estimate for θ . This algorithm is based on the ECM algorithm for partially nonlinear models by Ferreira, Borelli Zeller, and de Oliveira Garcia (2023), but incorporates a set of modifications to fit our assumed penalized log-likelihood. Specifically, we exclude the additional linear regression term and model the scale parameter through splines rather than linear regression, which introduces an additional penalty κ . Moreover, the parameters α and κ are assumed to be fixed. Ferreira and Paula (2017) show that the skew-normal density from Eq. (2) can be written in terms of a positive latent variable V through

$$p(y | \xi, \omega, \lambda) = 2\phi(y; \xi, \omega^2) \int_0^{+\infty} \phi(v; \lambda(y - \xi), \omega) dv,$$

where $\phi(x; \mu, \sigma^2)$ denotes the $\mathcal{N}(\mu, \sigma^2)$ pdf evaluated at x . The joint pdf of Y and V is then given by

$$p(y, v | \xi, \omega, \lambda) = 2\phi(y; \xi, \omega) \phi(v; \lambda(y - \xi), \omega). \quad (5)$$

It follows that $V|Y = y \sim TN(\lambda(y - \xi), \omega^2, 0, +\infty)$, where TN denotes the truncated normal distribution with parameters $\lambda(y - \xi)$ and ω^2 and support $(0, +\infty)$ (Johnson, Kotz, and Balakrishnan 1995). Due to Eq. (5), the complete data

log-likelihood for \mathbf{y} and the latent $\mathbf{v} = (v_1, \dots, v_n)^T$ satisfying the cause-effect model from Eq. (3) is given by

$$\begin{aligned} \ell_c(\theta | \mathbf{y}, \mathbf{v}) = & -n \log(\pi) - \sum_{i=1}^n \mathbf{z}_i^\top \boldsymbol{\rho} + \lambda \sum_{i=1}^n \frac{y_i - \mathbf{n}_i^\top \boldsymbol{\psi}}{\exp(\mathbf{z}_i^\top \boldsymbol{\rho})} v_i \\ & - \frac{1 + \lambda^2}{2} \sum_{i=1}^n \frac{(y_i - \mathbf{n}_i^\top \boldsymbol{\psi})^2}{\exp(\mathbf{z}_i^\top \boldsymbol{\rho})} - \frac{1}{2} \sum_{i=1}^n \frac{v_i^2}{\exp(\mathbf{z}_i^\top \boldsymbol{\rho})}. \end{aligned}$$

Based on $\hat{\boldsymbol{\theta}}^{(k)} = ((\hat{\boldsymbol{\psi}}^{(k)})^\top, (\hat{\boldsymbol{\rho}}^{(k)})^\top, \hat{\lambda}^{(k)})^\top$, denoting the parameter estimates after k iterations, further define

$$\begin{aligned} \hat{\mathbf{v}}^{(k)} &= (\hat{v}_1^{(k)}, \dots, \hat{v}_n^{(k)})^\top, & \hat{v}_i^{(k)} &= \mathbb{E} \left[V_i | Y_i, \hat{\boldsymbol{\theta}}^{(k)} \right], \\ \hat{\mathbf{v}}^2^{(k)} &= (\hat{v}_1^2^{(k)}, \dots, \hat{v}_n^2^{(k)})^\top, & \hat{v}_i^2^{(k)} &= \mathbb{E} \left[V_i^2 | Y_i, \hat{\boldsymbol{\theta}}^{(k)} \right]. \end{aligned}$$

Then, given $\hat{\boldsymbol{\theta}}^{(k)}$, the Q -function is computed as

$$\begin{aligned} Q(\theta | \hat{\boldsymbol{\theta}}^{(k)}) &= \mathbb{E} \left[\ell_c(\theta | \mathbf{y}, \mathbf{v}) | \mathbf{y}, \hat{\boldsymbol{\theta}}^{(k)} \right] \\ &\propto - \sum_{i=1}^n \mathbf{z}_i^\top \boldsymbol{\rho} - \frac{1}{2} \mathbf{1}_n^\top \mathbf{H} \hat{\mathbf{v}}^2^{(k)} + \lambda (\mathbf{y} - \mathbf{N}\boldsymbol{\psi})^\top \mathbf{H} \hat{\mathbf{v}}^{(k)} \\ &\quad - \frac{1 + \lambda^2}{2} (\mathbf{y} - \mathbf{N}\boldsymbol{\psi})^\top \mathbf{H} (\mathbf{y} - \mathbf{N}\boldsymbol{\psi}), \end{aligned}$$

where $\mathbf{H} = \text{diag}(\omega_1^{-2}, \dots, \omega_n^{-2})$ with $\omega_i = \exp(0.5 \mathbf{z}_i^\top \boldsymbol{\rho})$. The expectation is taken with respect to the conditional density $\mathbf{V} | \mathbf{Y} = \mathbf{y}$. In order to obtain the penalized maximum likelihood estimate w.r.t. Eq. (4), the quantity

$$Q_p(\theta | \hat{\boldsymbol{\theta}}^{(k)}) = Q(\theta | \hat{\boldsymbol{\theta}}^{(k)}) - \frac{\alpha}{2} \boldsymbol{\psi}^\top \mathbf{K} \boldsymbol{\psi} - \frac{\kappa}{2} \boldsymbol{\rho}^\top \mathbf{M} \boldsymbol{\rho}$$

is maximized by iteratively performing the following E-step and CM-steps. For the second CM-step, there is no analytical solution, so that we use the CMA-ES for maximization.

1) E-step: Given \mathbf{y} and the current estimates $\hat{\boldsymbol{\theta}}^{(k)}$, compute the conditional expectations of the latent variables appearing in the Q -function:

$$\begin{aligned} \hat{v}_i^{(k)} &= \hat{\lambda}^{(k)} e_i^{(k)} + \hat{\omega}_i^{(k)} W_\Phi \left(\frac{\hat{\lambda}^{(k)} e_i^{(k)}}{\hat{\omega}_i^{(k)}} \right), \\ \hat{v}_i^2^{(k)} &= \left(\hat{\lambda}^{(k)} e_i^{(k)} \right)^2 + \left(\hat{\omega}_i^{(k)} \right)^2 \\ &\quad + \hat{\lambda}^{(k)} e_i^{(k)} \hat{\omega}_i^{(k)} W_\Phi \left(\frac{\hat{\lambda}^{(k)} e_i^{(k)}}{\hat{\omega}_i^{(k)}} \right), \end{aligned}$$

where $e_i^{(k)} = y_i - \mathbf{n}_i^\top \hat{\boldsymbol{\psi}}^{(k)}$ and $W_\Phi(u) = \phi(u)(\Phi(u))^{-1}$.

2) CM-step 1: Fixing $\hat{\boldsymbol{\rho}}^{(k)}$, update $\hat{\boldsymbol{\psi}}^{(k)}$ and $\hat{\lambda}^{(k)}$ as

$$\begin{aligned} \hat{\boldsymbol{\psi}}^{(k+1)} &= \left(\mathbf{N}^\top \hat{\mathbf{H}}^{(k)} \mathbf{N} + \frac{\alpha}{1 + (\hat{\lambda}^{(k)})^2} \mathbf{K} \right)^{-1} \mathbf{N}^\top \hat{\mathbf{H}}^{(k)} \\ &\quad \cdot \left(\mathbf{y} - \frac{\hat{\lambda}^{(k)}}{1 + (\hat{\lambda}^{(k)})^2} \hat{\mathbf{v}}^{(k)} \right), \\ \hat{\lambda}^{(k+1)} &= \frac{\left(\mathbf{y} - \mathbf{N} \hat{\boldsymbol{\psi}}^{(k)} \right)^\top \hat{\mathbf{H}}^{(k)} \hat{\mathbf{v}}^{(k)}}{\left(\mathbf{y} - \mathbf{N} \hat{\boldsymbol{\psi}}^{(k)} \right)^\top \hat{\mathbf{H}}^{(k)} \left(\mathbf{y} - \mathbf{N} \hat{\boldsymbol{\psi}}^{(k)} \right)}. \end{aligned}$$

3) CM-step 2: Given $\hat{\psi}^{(k+1)}$ and $\hat{\lambda}^{(k+1)}$, update $\hat{\rho}^{(k)}$ as

$$\hat{\rho}^{(k+1)} = \operatorname{argmax}_{\rho} Q_{\rho}(\rho | \hat{\psi}^{(k+1)}, \hat{\lambda}^{(k+1)}).$$

The algorithm stops if $\|\hat{\theta}^{(k+1)} - \hat{\theta}^{(k)}\|_2 < 10^{-6}$ or after a specified maximum number of iterations. Having obtained refined parameter estimates in both directions, our method proceeds to infer the causal direction.

4 Cause-Effect Inference with SKEWD

To distinguish cause and effect based on the iid samples $(x_1, y_1), \dots, (x_n, y_n)$, SKEWD, short for *skewness-robust discovery*, fits skew-normal LSNMs $X \rightarrow Y$ and $Y \rightarrow X$ based on Algorithm 1. Given the estimated models, SKEWD performs cause-effect inference through independence testing or likelihood scoring, as common in prior works.

Independence Testing Regression with subsequent independence testing (Peters et al. 2014) is a widely used causal discovery approach. The cause-effect inference is based on the independence between cause and noise in the assumed model. Under the modeling assumptions, X and N_Y should be independent in LSNM $X \rightarrow Y$, and analogously, Y and N_X should be independent in LSNM $Y \rightarrow X$. The estimated noise variables are extracted through the equations

$$\hat{N}_Y = \frac{Y - \hat{f}_{X \rightarrow Y}(X)}{\hat{g}_{X \rightarrow Y}(X)} \text{ and } \hat{N}_X = \frac{X - \hat{f}_{Y \rightarrow X}(Y)}{\hat{g}_{Y \rightarrow X}(Y)}.$$

Subsequently, independence tests are performed for the cause-noise pair in each direction. SKEWD uses the HSIC test (Gretton et al. 2005) and infers the direction with the higher p -value due to higher evidence for independence. Fig. 1 illustrates the noise extraction in the true causal direction of a simulated data pair. The full example including the reverse direction is provided in Appendix B.

Likelihood Scoring To perform cause-effect inference via likelihood scoring, SKEWD determines the direction by evaluating the joint log-likelihoods $\ell_{X \rightarrow Y}$ and $\ell_{Y \rightarrow X}$, where

$$\ell_{X \rightarrow Y}(\mathbf{x}, \mathbf{y}) = \log(p(\mathbf{x})) + \log(p_{X \rightarrow Y}(\mathbf{y}|\mathbf{x}))$$

and $\ell_{Y \rightarrow X}$ is given analogously. The direction with the higher estimated log-likelihood is inferred by SKEWD. An estimate for $p_{X \rightarrow Y}(\mathbf{y}|\mathbf{x})$, the conditional density of $\mathbf{Y}|\mathbf{X}$ in direction $X \rightarrow Y$, is obtained by estimating the corresponding skew-normal LSNM. SKEWD with likelihood scoring assumes that the observations of X and Y have been standardized to avoid potential biases due to scaling (Reisach, Seiler, and Weichwald 2021). It further assumes that the marginal distributions of X and Y are normal distributions. As shown in Appendix A, in that case, the marginal log-likelihoods can be considered equal and hence be neglected.

Notes on Identifiability The previously discussed cause-effect inference through independence testing or likelihood scoring is only valid if identifiability holds under the skew-normal LSNM. Strobl and Lasko (2023) and Immer et al. (2023) have shown that the causal direction in general LSNMs is identifiable, unless a specific ordinary differential

equation is satisfied. This includes the skew-normal LSNM, so that identifiability should hold apart from pathological cases. We note that the derived result, which we provide in Appendix A for completeness, requires that the conditional log-densities $\log(p_{X \rightarrow Y}(\mathbf{y}|\mathbf{x}))$ and $\log(p_{Y \rightarrow X}(\mathbf{x}|\mathbf{y}))$ are two-times differentiable. This condition is satisfied for the skew-normal LSNM.

5 Related Work

We discuss related work for (bivariate) causal discovery, and the parameter estimation for skew-normal distributions.

Causal Discovery Identification results for a variety of function classes have been derived, including additive noise models (ANMs) (Shimizu et al. 2006; Hoyer et al. 2008; Bühlmann, Peters, and Ernest 2014), post-nonlinear additive noise models (PNL) (Zhang and Hyvärinen 2009; Zhang et al. 2015; Uemura et al. 2022), and location-scale noise models (LSNMs) (Khemakhem et al. 2021; Xu et al. 2022; Immer et al. 2023; Strobl and Lasko 2023), where PNL and LSNMs are both generalizations of ANMs. Besides those approaches, some works focus on low-noise distributions (almost deterministic) in the context of ANMs (Janzing et al. 2012; Blöbaum et al. 2018), and LSNMs (Xu et al. 2022; Cai et al. 2020). Another body of work aims to exploit the postulate that the mechanism ($p_{Y|X}$) is independent of the cause (p_X), whereas this does not hold for the anti-causal direction (Peters, Janzing, and Schölkopf 2017, Ch. 2). One approach is to estimate the involved distributions directly (Sgouritsa et al. 2015; Goulet et al. 2018), or via Bayesian model selection (Dhir, Power, and Van Der Wilk 2024). A different line of work is motivated through the information-theoretic variant of this principle, the algorithmic Markov condition (Janzing and Schölkopf 2010), which is formulated through Kolmogorov complexity, and can be linked to two-part coding (Marx and Vreeken 2022). Practical approaches approximate the postulate via the minimum message length or minimum description length principle (Mooij et al. 2010; Marx and Vreeken 2017; Kalainathan 2019; Tagasovska, Chavez-Demoulin, and Vatter 2020; Mian, Marx, and Vreeken 2021).

We here focus on LSNMs, since they are a rather general model class, for which general identification results exist (Immer et al. 2023; Strobl and Lasko 2023), which imply that LSNMs are identifiable in most cases. However, in comparison to ANMs and PNL, an exhaustive enumeration of non-identifiable cases does not exist. Nonetheless, for Gaussian noise (Khemakhem et al. 2021), exponential family models (Bodik and Chavez-Demoulin 2025), uniform and continuous Bernoulli (Sun and Schulte 2023), the non-identifiable cases have been characterized. Another approach, which builds upon the identification result of LOCI (Immer et al. 2023), relaxes the Gaussianity assumption for the parameter estimation is ROCHE (Tran et al. 2024), where the authors model the noise distribution via Student’s t -distribution, which allows for modeling of different tail behavior. Some of the approaches above have also been extended to graphs with more than two nodes (Duong and Nguyen 2023; Kamkari et al. 2024). Notably, Lin et al.

(2024) focus on symmetric noise distributions and show how, under this assumption, skewness will appear in the anti-causal model, which allows them to derive a score-based method. In contrast, we explicitly model the skewness of the noise variable for which we develop both an independence-based and a likelihood-based approach.

Skew-Normal The skew-normal distribution (Azzalini 1985) is a popular choice for modeling skewness, though maximum likelihood estimation is challenging. As noted by Azzalini and Arellano-Valle (2013), the skew-normal likelihood may lack a finite maximum, which can be addressed by including a penalty term with specific properties. Another difficulty is the presence of a stationary point at $\lambda = 0$ when considering the parameterization as defined in Eq. (2). To circumvent this problem, maximization can be carried out with respect to a reparameterization of the skew-normal (Azzalini 1985). Moreover, EM algorithms (Azzalini 2013) and genetic algorithms have been considered (Yaçınkaya, Şenoğlu, and Yolcu 2018). In statistical modeling, EM algorithms are often used. For example, Arellano-Valle, Bolfarine, and Lachos (2005) apply an EM algorithm to linear mixed models, noting that direct iterative maximization may cause computational problems and is less robust to starting values. Ferreira and Paula (2017) considered an EM algorithm for partially linear models. Ferreira, Borelli Zeller, and de Oliveira Garcia (2023) extended this work to an ECM algorithm for heteroscedastic partially linear models. We adapt their approach by modeling the scale parameter through penalized splines while removing the linear regression term, and we use it to improve the result of our heuristic optimization.

6 Experiments

We evaluate SKEWD with likelihood scoring (SKEWD-LL) and independence testing (SKEWD-IT) on established bivariate causal discovery benchmarks and novel synthetic LSNM datasets that exhibit varying degrees of skewness. We compare the performance in terms of accuracy and area under the decision rate curve (AUDRC) against different state-of-the-art methods for bivariate causal discovery. The AUDRC measures how well the certainty of an algorithm coincides with its accuracy (Marx and Vreeken 2019; Immer et al. 2023). For SKEWD, higher certainty corresponds to a larger absolute difference in the log-likelihoods or the p -values from independence tests. The AUDRC is computed by sorting predictions from most to least certain and averaging the accuracies over the top m predictions for $m = 1, \dots, M$, where M is the number of pairs. Let $\pi(i)$ be the index of the i -th most certain prediction, $f(\pi(i))$ the predicted direction and $t(\pi(i))$ the correct direction, then

$$\text{AUDRC} = \frac{1}{M} \sum_{m=1}^M \frac{1}{m} \sum_{i=1}^m \mathbb{1}[f(\pi(i)) = t(\pi(i))].$$

As with accuracy, the AUDRC is bounded by 0 and 1, with larger values reflecting better performance.

Baselines We include LOCI (Immer et al. 2023), ROCHE (Tran et al. 2024), GRCI (Strobl and Lasko 2023)

and QCCD (Tagasovska, Chavez-Demoulin, and Vatter 2020) as LSNM-specific approaches. For LOCI, which assumes normally distributed noise, we consider both proposed log-likelihood and independence test versions, LOCI-LL and LOCI-IT, with neural network estimators. ROCHE assumes t -distributed noise, and GRCI extracts residuals via cross-validated regression (both are independence-test-based). QCCD computes scores via quantile regression. We further include CAM (Bühlmann, Peters, and Ernest 2014) and RESIT (Peters et al. 2014) which assume ANMs. Lastly, we consider IGCI (Janzing et al. 2012) and IGCI with prior standardization (IGCI-G).

Skew-Noise Datasets To create LSNM (and ANM) datasets with skewed noise, we base our approach on the data-generating mechanisms used by Tagasovska, Chavez-Demoulin, and Vatter (2020). That is, we generate ANMs of the form $Y = f(X) + \varepsilon$ and LSNMs of the form $Y = f(X) + g(X)\varepsilon$, where f, g are randomly sampled sigmoidal functions as in the original ANs and LSs datasets. The resulting injective functions pose a more challenging cause-effect inference than randomly generated potentially non-invertible functions. The distribution of the cause is hierarchically defined by $X \sim \mathcal{N}(0, \sigma^2)$, where $\sigma^2 \sim U[1, 2]$. For the noise source, we differentiate five cases. We consider two parameterizations of the skew-normal distribution, with $\varepsilon \sim \text{SN}(0, 1, \lambda)$ where $\lambda \in \{-2, 20\}$. Additionally, we consider three parameterizations of the generalized normal (GNO) distribution (Hosking 1986) with $\varepsilon \sim \text{GNO}(0, 1, k)$, where the shape parameter k is varied between 0.15, -0.31 , and -0.5 . The GNO distribution is a reparametrized three-parameter lognormal distribution (Kozlov and Maysuradze 2019) that generalizes the normal distribution and can exhibit higher levels of skewness than the skew-normal distribution. More details on the GNO distribution are provided in Appendix A.

For each case, we sample 100 pairs with 1000 observations each across the ANs and LSs setting. For our analysis, we combine the skew-normal datasets with $\lambda = -2$ and GNO datasets with $\kappa = 0.15$ into one dataset class, since they both exhibit roughly the same skewness ($\gamma_1 \approx -0.455$). Similarly, we group together the datasets with $\lambda = 20$ and $\kappa = -0.31$, both expressing a skewness of $\gamma_1 \approx 0.985$. The $\text{GNO}(0, 1, -0.5)$ distribution yields a higher skewness $\gamma_1 \approx 1.750$ than what can be modeled by the skew-normal distribution. For reference, the exponential distribution always exhibits a skewness of 2. We denote the resulting datasets in correspondence to the specific skewness level γ_1 as ANs(γ_1) and LSs(γ_1). Scatter plots of data pairs from each generated dataset are provided in Appendix C.

Established Benchmark Datasets We consider several established benchmarks to investigate the general applicability of SKEWD. These include the original AN, ANs, LS, LSs and MNU dataset featuring multiplicative noise from Tagasovska, Chavez-Demoulin, and Vatter (2020). We also consider the synthetic SIM, SIMc (includes confounding), SIMln (low noise), SIMG (near Gaussian ANM) datasets as well as the real-world Tübingen benchmark (Mooij et al. 2016). Multivariate and discrete data were removed from the

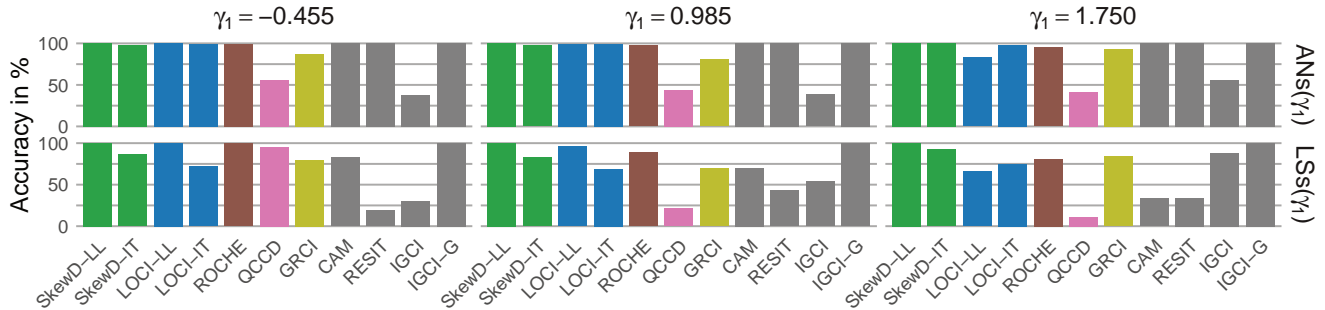


Figure 2: Accuracy in % for SKEWD and the baselines (approaches not developed for LSNMs in gray) on the proposed ANs and LSs datasets with skewness levels -0.455 , 0.985 and 1.750 . SKEWD consistently performs well, whereas the likelihood-based variant shows the strongest performance. IGCI-G while strongly misspecified seems to be biased toward the correct direction.

Tübingen benchmark, resulting in 99 pairs. Lastly, we include the Cha (used in the cause-effect pair challenge), Net (generated from random neural networks) and Multi datasets (generated from polynomial mechanisms) (Guyon, Statnikov, and Batu 2019), resulting in 13 additional datasets.

Results Under Skewed Noise In Fig. 2 we plot the accuracy of SKEWD and all baselines when applied to the proposed skew-noise datasets. We supplement the exact values for both accuracy and AUDRC in Appendix B. As the results for both metrics are consistent, we focus the discussion on accuracy. Notably, SKEWD-LL is the only method to achieve perfect accuracy across all cases and outperforms SKEWD-IT, especially in the LSs setting. IGCI-G demonstrates comparable performance, making only a single error across all datasets, although IGCI-G is highly misspecified, since it assumes almost deterministic functions. Among the LSNM-specific methods, ROCHE is the most reliable aside from SKEWD. However, its performance degrades in increasingly skewed LSNM settings, dropping to 81% accuracy for LSs(1.750). Similarly, as expected, both versions of LOCI and QCCD exhibit decreasing accuracy under increased skewness with QCCD becoming severely biased towards the false direction in the LSs case. The ANM-specific methods CAM and RESIT show robustness towards skewed ANMs, but their accuracy drops for LSNMs.

Results for Established Benchmarks We summarize the performances of all baselines in terms of mean accuracy and AUDRC across all 13 established benchmarks in Tab. 1 including the respective standard deviations. The results demonstrate that SKEWD performs competitively. SKEWD-IT ranks second with a difference of 2.67% in accuracy to ROCHE, which is expected to have an advantage to our approach when distributions are heavy-tailed. Compared to LOCI, the larger model class that we consider shows a slight advantage on the established benchmarks and a strong advantage on the proposed skewed benchmarks as discussed in the previous section. Further, our results confirm the observations made by previous approaches (Immer et al. 2023; Sun and Schulte 2023) that methods based on subsequent independence testing (in our case SKEWD-IT) are more robust across various settings.

Method	Accuracy (%) \uparrow	AUDRC (%) \uparrow
SKEWD-LL	77.43 \pm 20.56	84.77 \pm 17.87
SKEWD-IT	85.02 \pm 9.71	91.65 \pm 9.32
LOCI-LL	77.08 \pm 22.22	84.65 \pm 18.54
LOCI-IT	84.09 \pm 12.20	89.51 \pm 12.74
ROCHE	87.69 \pm 10.65	92.90 \pm 8.40
QCCD	78.21 \pm 17.29	85.77 \pm 14.26
GRCI	83.20 \pm 9.82	89.77 \pm 10.54
CAM	72.42 \pm 22.10	73.85 \pm 22.87
RESIT	61.85 \pm 32.62	66.25 \pm 31.68
IGCI	46.36 \pm 20.66	49.60 \pm 24.74
IGCI-G	73.69 \pm 23.92	77.21 \pm 25.04

Table 1: Mean and standard deviation of accuracy, AUDRC over all 13 established benchmarks. Top two are bolded.

In addition to the above analysis, we provide the individual results for each dataset in Appendix B. Most notably, with 88% accuracy on SIMG, SKEWD-LL outperforms all remaining methods in terms of accuracy by at least 5%. Over the original AN, ANs, LS, and LSs datasets with normally distributed noise, SKEWD-LL scores perfect accuracy demonstrating its effectiveness under symmetric and skewed noise. We also compute the mean accuracy across all 19 datasets (including our novel datasets), for which SKEWD-LL improves to 84.56%, and SKEWD-IT to 87.46%.

7 Conclusion

In this paper, we focused on bivariate causal discovery under skewed noise distributions. We proposed a set of novel skew-noise datasets, based on which we demonstrated that state-of-the-art (SOTA) methods for location-scale noise models become unreliable under increasingly skewed noise. To address this issue we proposed SKEWD, which performs cause-effect inference based on independence testing or likelihood scoring under the assumption of skew-normally distributed noise. For parameter estimation, we devised a novel estimation approach for skew-normal LSNMs which refines an estimate of a heuristic search via an ECM algorithm. Our results show that SKEWD is, in contrast to SOTA,

robust with respect to higher amounts of skewness while performing on par with SOTA on established benchmarks.

Limitations and Future Work Despite showing promising results, there are a few limitations that we would like to work on in the future. Natural extensions of our work would be to consider multivariate cause-effect inference, extensions to also consider heavy tailed distributions, or lifting the Gaussianity assumption of the marginals for the likelihood-based approach, e.g., by considering kernel density estimation or normalizing flows.

Acknowledgements The authors would like to thank Clécio da Silva Ferreira for supporting this work by generously providing code and valuable insights. They also gratefully acknowledge the computing time provided on the Linux HPC cluster at Technical University Dortmund (LiDO3), partially funded in the course of the Large-Scale Equipment Initiative by the Deutsche Forschungsgemeinschaft (DFG, German Research Foundation) as project 271512359.

References

- Arellano-Valle, R. B.; Bolfarine, H.; and Lachos, V. H. 2005. Skew-Normal Linear Mixed Models. *Journal of Data Science*, 3: 415–438.
- Azzalini, A. 1985. A Class of Distributions Which Includes the Normal Ones. *Scandinavian Journal of Statistics*, 12(2): 171–178.
- Azzalini, A. 2013. *The Skew-Normal and Related Families*, volume 3. Cambridge University Press.
- Azzalini, A.; and Arellano-Valle, R. B. 2013. Maximum Penalized Likelihood Estimation for Skew-Normal and Skew-t Distributions. *Journal of Statistical Planning and Inference*, 143(2): 419–433.
- Blöbaum, P.; Janzing, D.; Washio, T.; Shimizu, S.; and Schölkopf, B. 2018. Cause-Effect Inference by Comparing Regression Errors. In *International Conference on Artificial Intelligence and Statistics*, 900–909. PMLR.
- Bodik, J.; and Chavez-Demoulin, V. 2025. Identifiability of Causal Graphs Under Nonadditive Conditionally Parametric Causal Models. arXiv:2303.15376.
- Bühlmann, P.; Peters, J.; and Ernest, J. 2014. CAM: Causal Additive Models, High-Dimensional Order Search and Penalized Regression. *The Annals of Statistics*, 42(6): 2526–2556.
- Cai, R.; Ye, J.; Qiao, J.; Fu, H.; and Hao, Z. 2020. FOM: Fourth-Order Moment based Causal Direction Identification on the Heteroscedastic Data. *Neural Networks*, 124: 193–201.
- Chickering, D. M. 2002. Optimal Structure Identification with Greedy Search. *Journal of Machine Learning Research*, 3(Nov): 507–554.
- Dempster, A. P.; Laird, N. M.; and Rubin, D. B. 1977. Maximum Likelihood from Incomplete Data via the EM Algorithm. *Journal of the Royal Statistical Society: Series B (Methodological)*, 39(1): 1–22.
- Dhir, A.; Power, S.; and Van Der Wilk, M. 2024. Bivariate Causal Discovery using Bayesian Model Selection. In *Proceedings of the 41st International Conference on Machine Learning*, 10710–10735.
- Duong, B.; and Nguyen, T. 2023. Heteroscedastic Causal Structure Learning. In *ECAI 2023*, 598–605. IOS Press.
- Eilers, P. H. C.; and Marx, B. D. 1996. Flexible Smoothing with B-Splines and Penalties. *Statistical Science*, 11(2): 89–121.
- Ferreira, C. S.; Borelli Zeller, C.; and de Oliveira Garcia, R. R. 2023. Heteroscedastic Partially Linear Model Under Skew-Normal Distribution with Application in Ragweed Pollen Concentration. *Journal of Applied Statistics*, 50(6): 1255–1282.
- Ferreira, C. S.; and Paula, G. A. 2017. Estimation and Diagnostic for Skew-Normal Partially Linear Models. *Journal of Applied Statistics*, 44(16): 3033–3053.
- Frazier, P. I. 2018. A Tutorial on Bayesian Optimization. arXiv:1807.02811.
- Genton, M. G., ed. 2004. *Skew-Elliptical Distributions and Their Applications: A Journey Beyond Normality*. Chapman and Hall/CRC, 1 edition.
- Goudet, O.; Kalainathan, D.; Caillou, P.; Guyon, I.; Lopez-Paz, D.; and Sebag, M. 2018. Learning Functional Causal Models with Generative Neural Networks. *Explainable and Interpretable Models in Computer Vision and Machine Learning*, 39.
- Green, P. J. 1990. On Use of the EM Algorithm for Penalized Likelihood Estimation. *Journal of the Royal Statistical Society Series B: Statistical Methodology*, 52(3): 443–452.
- Gretton, A.; Bousquet, O.; Smola, A.; and Schölkopf, B. 2005. Measuring Statistical Dependence with Hilbert-Schmidt Norms. In *International Conference on Algorithmic Learning Theory*, 63–77. Springer.
- Guyon, I.; Statnikov, A.; and Batu, B. B. 2019. *Cause effect pairs in machine learning*. Springer.
- Hansen, N. 2023. The CMA Evolution Strategy: A Tutorial. arXiv:1604.00772.
- Hansen, N.; and Ostermeier, A. 2001. Completely Derandomized Self-Adaptation in Evolution Strategies. *Evolutionary Computation*, 9(2): 159–195.
- Hosking, J. R. M. 1986. The Theory of Probability Weighted Moments. Technical report, IBM Research Division, Thomas J. Watson Research Center, New York.
- Hoyer, P. O.; Janzing, D.; Mooij, J. M.; Peters, J.; and Schölkopf, B. 2008. Nonlinear Causal Discovery with Additive Noise Models. In *Advances in Neural Information Processing Systems*, volume 21.
- Immer, A.; Schultheiss, C.; Vogt, J. E.; Schölkopf, B.; Bühlmann, P.; and Marx, A. 2023. On the Identifiability and Estimation of Causal Location-Scale Noise Models. In *International Conference on Machine Learning*, 14316–14332. PMLR.
- Janzing, D.; Mooij, J.; Zhang, K.; Lemeire, J.; Zscheischler, J.; Daniušis, P.; Steudel, B.; and Schölkopf, B. 2012.

- Information-Geometric Approach to Inferring Causal Directions. *Artificial Intelligence*, 182: 1–31.
- Janzing, D.; and Schölkopf, B. 2010. Causal Inference Using the Algorithmic Markov Condition. *IEEE Transactions on Information Theory*, 56(10): 5168–5194.
- Johnson, N. L.; Kotz, S.; and Balakrishnan, N. 1995. *Continuous Univariate Distributions*, volume 2. John Wiley & Sons.
- Kalainathan, D. 2019. *Generative Neural Networks to infer Causal Mechanisms: algorithms and applications*. Ph.D. thesis, Université Paris-Saclay.
- Kamkari, H.; Balazadeh, V.; Zehtab, V.; and Krishnan, R. G. 2024. Order-Based Structure Learning with Normalizing Flows. arXiv:2308.07480.
- Karlis, D.; and Xekalaki, E. 2003. Choosing Initial Values for the EM Algorithm for Finite Mixtures. *Computational Statistics & Data Analysis*, 41(3-4): 577–590.
- Khemakhem, I.; Monti, R.; Leech, R.; and Hyvarinen, A. 2021. Causal Autoregressive Flows. In *International Conference on Artificial Intelligence and Statistics*, 3520–3528. PMLR.
- Kozlov, V.; and Maysuradze, A. 2019. Parameter Estimation in a Three-Parameter Lognormal Distribution. *Computational Mathematics and Modeling*, 30(3): 302–310.
- Kozubowski, T.; and Podgorski, K. 2000. A Multivariate and Asymmetric Generalization of Laplace Distribution. *Computational Statistics*, 15: 531–540.
- Lin, Y.; Huang, Y.; Liu, W.; Deng, H.; Ng, I.; Zhang, K.; Gong, M.; Ma, Y.-A.; and Huang, B. 2024. A Skewness-Based Criterion for Addressing Heteroscedastic Noise in Causal Discovery. In *International Conference on Learning Representations*.
- Marx, A.; and Vreeken, J. 2017. Telling Cause From Effect Using MDL-Based Local and Global Regression. In *2017 IEEE international conference on data mining (ICDM)*, 307–316. IEEE.
- Marx, A.; and Vreeken, J. 2019. Telling Cause from Effect by Local and Global Regression. *Knowledge and Information Systems*, 60(3): 1277–1305.
- Marx, A.; and Vreeken, J. 2022. Formally Justifying MDL-based Inference of Cause and Effect. In *AAAI Workshop on Information-Theoretic Causal Inference and Discovery (ITCI'22)*.
- Meng, X.-L.; and Rubin, D. B. 1993. Maximum Likelihood Estimation via the ECM Algorithm: A General Framework. *Biometrika*, 80(2): 267–278.
- Mian, O.; Marx, A.; and Vreeken, J. 2021. Discovering Fully Oriented Causal Networks. In *Proceedings of the AAAI Conference on Artificial Intelligence*, volume 35, 8975–8982.
- Mooij, J. M.; Peters, J.; Janzing, D.; Zscheischler, J.; and Schölkopf, B. 2016. Distinguishing Cause from Effect Using Observational Data: Methods and Benchmarks. *The Journal of Machine Learning Research*, 17(1): 1103–1204.
- Mooij, J. M.; Stegle, O.; Janzing, D.; Zhang, K.; and Schölkopf, B. 2010. Probabilistic Latent Variable Models for Distinguishing Between Cause and Effect. In *Proceedings of the 24th International Conference on Neural Information Processing Systems - Volume 2*, 1687–1695.
- Nomura, M.; and Shibata, M. 2024. cmaes : A Simple yet Practical Python Library for CMA-ES. arXiv:2402.01373.
- Peters, J.; Janzing, D.; and Schölkopf, B. 2017. *Elements of Causal Inference: Foundations and Learning Algorithms*. The MIT Press.
- Peters, J.; Mooij, J. M.; Janzing, D.; and Schölkopf, B. 2014. Causal Discovery with Continuous Additive Noise Models. *Journal of Machine Learning Research*, 15(1): 2009–2053.
- Ramsey, J.; Hanson, S.; Hanson, C.; Halchenko, Y.; Poldrack, R.; and Glymour, C. 2010. Six Problems for Causal Inference from fMRI. *NeuroImage*, 49(2): 1545–1558.
- Reisach, A.; Seiler, C.; and Weichwald, S. 2021. Beware of the Simulated DAG! Causal Discovery Benchmarks May Be Easy to Game. In *Proceedings of the 35th International Conference on Neural Information Processing Systems*.
- Runge, J.; Bathiany, S.; Bollt, E.; Camps-Valls, G.; Coumou, D.; Deyle, E.; Glymour, C.; Kretschmer, M.; Mahecha, M. D.; Muñoz-Marí, J.; van Nes, E. H.; Peters, J.; Quax, R.; Reichstein, M.; Scheffer, M.; Schölkopf, B.; Spirtes, P.; Sugihara, G.; Sun, J.; Zhang, K.; and Zscheischler, J. 2019. Inferring Causation from Time Series in Earth System Sciences. *Nature Communications*, 10(1): 2553.
- Schultheiss, C.; and Bühlmann, P. 2023. On the Pitfalls of Gaussian Likelihood Scoring for Causal Discovery. *Journal of Causal Inference*, 11(1): 20220068.
- Sgouritsa, E.; Janzing, D.; Hennig, P.; and Schölkopf, B. 2015. Inference of Cause and Effect with Unsupervised Inverse Regression. In *Proceedings of the 18th International Conference on Artificial Intelligence and Statistics*, volume 38 of *JMLR Workshop and Conference Proceedings*, 847–855.
- Shimizu, S.; Hoyer, P. O.; Hyvärinen, A.; Kerminen, A.; and Jordan, M. 2006. A Linear Non-Gaussian Acyclic Model for Causal Discovery. *Journal of Machine Learning Research*, 7(10).
- Spirtes, P.; Glymour, C. N.; and Scheines, R. 2000. *Causation, Prediction, and Search*. MIT press.
- Strobl, E. V.; and Lasko, T. A. 2023. Identifying Patient-Specific Root Causes with the Heteroscedastic Noise Model. *Journal of Computational Science*, 72: 102099.
- Sun, X.; and Schulte, O. 2023. Cause-Effect Inference in Location-Scale Noise Models: Maximum Likelihood vs. Independence Testing. In *Conference on Neural Information Processing Systems*.
- Tagasovska, N.; Chavez-Demoulin, V.; and Vatter, T. 2020. Distinguishing Cause from Effect Using Quantiles: Bivariate Quantile Causal Discovery. In *International Conference on Machine Learning*, 9311–9323. PMLR.
- Tran, Q.-D.; Duong, B.; Nguyen, P.; and Nguyen, T. 2024. Robust Estimation of Causal Heteroscedastic Noise Models. In *Proceedings of the 2024 SIAM International Conference on Data Mining (SDM)*, 788–796. SIAM.

Uemura, K.; Takagi, T.; Takayuki, K.; Yoshida, H.; and Shimizu, S. 2022. A Multivariate Causal Discovery based on Post-Nonlinear Model. In *Proceedings of the First Conference on Causal Learning and Reasoning*, volume 177 of *Proceedings of Machine Learning Research*, 826–839. PMLR.

Vuković, M.; and Thalmann, S. 2022. Causal Discovery in Manufacturing: A Structured Literature Review. *Journal of Manufacturing and Materials Processing*, 6(1): 10.

Xu, S.; Mian, O. A.; Marx, A.; and Vreeken, J. 2022. Inferring Cause and Effect in the Presence of Heteroscedastic Noise. In *International Conference on Machine Learning*, 24615–24630. PMLR.

Yalçınkaya, A.; Şenoğlu, B.; and Yolcu, U. 2018. Maximum Likelihood Estimation for the Parameters of Skew Normal Distribution Using Genetic Algorithm. *Swarm and Evolutionary Computation*, 38: 127–138.

Zhang, K.; and Hyvärinen, A. 2009. On the Identifiability of the Post-Nonlinear Causal Model. In *Proc. 25th Conference on Uncertainty in Artificial Intelligence (UAI2009)*, 647–655. AUAI Press.

Zhang, K.; Wang, Z.; Zhang, J.; and Schölkopf, B. 2015. On Estimation of Functional Causal Models: General Results and Application to the Post-Nonlinear Causal Model. *ACM Transactions on Intelligent Systems and Technology (TIST)*, 7(2): 1–22.

Appendix

A Technical Details

Skew-Distributions

In this section, we present more details on the considered skewed distributions, the skew-normal and the generalized normal. This includes their pdf, expected value, variance and skewness.

Skew-Normal As discussed in Sec. 2, the random variable X follows a univariate skew-normal distribution (Azzalini 1985) with parameters $\xi \in \mathbb{R}$ (location), $\omega > 0$ (scale), and $\lambda \in \mathbb{R}$ (shape), $X \sim \text{SN}(\xi, \omega, \lambda)$, if its probability density function (pdf) is given by

$$p(x) = \frac{2}{\omega} \phi\left(\frac{x - \xi}{\omega}\right) \Phi\left(\lambda \frac{x - \xi}{\omega}\right), \quad x \in \mathbb{R}.$$

Define $b = \sqrt{2/\pi}$ and $\delta = \lambda/\sqrt{(1 + \lambda^2)}$. Then, the expected value, the variance and the skewness of $X \sim \text{SN}(\xi, \omega, \lambda)$ are given by

$$\mathbb{E}[X] = \xi + \omega b \delta, \quad \text{Var}(X) = \omega^2(1 - b^2 \delta^2), \quad \text{and } \gamma_1 = \frac{4 - \pi}{2} \frac{b^3 \delta^3}{(1 - b^2 \delta^2)^{3/2}}.$$

The skew-normal distribution is right-skewed if $\lambda > 0$ and left-skewed if $\lambda < 0$ and its skewness is bounded by the interval $(-\gamma_1^{\max}, \gamma_1^{\max})$, where $\gamma_1^{\max} \approx 0.9953$. If $\lambda = 0$, the distribution corresponds to a normal distribution with mean ξ and variance ω^2 . We note that the location and scale parameter do not correspond to the mean and the standard deviation. In consequence, SKEWD does not directly model the mean and standard deviation via the functions f and g defined in the skew-normal LSNM in Section 2.

Generalized Normal The generalized normal (GNO) distribution (Hosking 1986) is a reparametrized version of the three-parameter lognormal distribution (see for instance Kozlov and Maysuradze (2019)). The random variable X follows a GNO distribution, $X \sim \text{GNO}(\xi, \alpha, k)$, if its pdf is given by

$$p(x) = \frac{1}{\sqrt{2\pi}} \frac{1}{\alpha} \exp(ky - 0.5y^2), \quad \text{where } y = \begin{cases} -\frac{1}{k} \log(1 - k \frac{x - \xi}{\alpha}) & , k \neq 0 \\ \frac{x - \xi}{\alpha} & , k = 0 \end{cases} \quad (6)$$

with support $\xi + \frac{\alpha}{k} \leq x < \infty$ if $k < 0$, $-\infty < x < \infty$ if $k = 0$, and $-\infty < x \leq \xi + \frac{\alpha}{k}$ if $k > 0$. It follows that the GNO distribution with $k = 0$, $X \sim \text{GNO}(\xi, \alpha, 0)$, corresponds to the regular normal distribution with mean ξ and variance α^2 . For $k \neq 0$, the mean and variance are given by

$$\mathbb{E}[X] = \xi - \frac{\alpha}{k} (\exp(0.5k^2) - 1), \quad \text{Var}(X) = \frac{\alpha^2}{k^2} \exp(k^2) (\exp(k^2) - 1)$$

and the skewness corresponds to

$$\gamma_1 = \text{sign}(k) \frac{3 \exp(k^2) - \exp(3k^2) - 2}{(\exp(k^2) - 1)^{3/2}}.$$

When $k < 0$ the GNO distribution has a lower bound and exhibits positive skewness, whereas when $k > 0$ the GNO distribution has an upper bound and exhibits negative skewness.

Neglection of Marginal Log-Likelihoods

When performing likelihood scoring with SKEWD, it is assumed that the cause is normally distributed and that the observations have been standardized for model estimation. We argue that in that case the marginal log-likelihoods $p(\mathbf{x})$, $p(\mathbf{y})$ of the hypothesized causes can be neglected. By Proposition 1 stated below, we can treat the standardized variables as approximately standard normal in large samples and thus model the marginal likelihoods via standard normal distributions. Let x_1, \dots, x_n denote the observed standardized causes with respect to SCM $X \rightarrow Y$. Then,

$$\log(p_{X \rightarrow Y}(\mathbf{x})) = \sum_{i=1}^n \log(\phi(x_i)) = -\frac{n}{2} \log(2\pi) - \frac{1}{2} \sum_{i=1}^n x_i^2 = -\frac{n}{2} \log(2\pi) - \frac{n-1}{2},$$

where the last equality stems from the fact that the sum of n squared standardized observations is equal to $n - 1$. To show this, let v_1, \dots, v_n denote the non-standardized observed causes and define $\bar{v} = \frac{1}{n} \sum_{j=1}^n v_j$ and $s = \sqrt{\frac{1}{n-1} \sum_{i=1}^n (v_i - \bar{v})^2}$. Then,

$$\sum_{i=1}^n x_i^2 = \sum_{i=1}^n \frac{(v_i - \bar{v})^2}{s^2} = \frac{\sum_{i=1}^n (v_i - \bar{v})^2}{\frac{1}{n-1} \sum_{i=1}^n (v_i - \bar{v})^2} = n - 1.$$

Analogously, we can approximate $\log(p_{Y \rightarrow X}(\mathbf{y}))$ and due to the equality of the marginal log-likelihoods neglect these two terms when comparing the model log-likelihoods

$$\ell_{X \rightarrow Y}(\mathbf{x}, \mathbf{y}) = \log(p(\mathbf{x})) + \log(p_{X \rightarrow Y}(\mathbf{y}|\mathbf{x})) \stackrel{\geq}{\approx} \log(p(\mathbf{y})) + \log(p_{Y \rightarrow X}(\mathbf{x}|\mathbf{y})) = \ell_{Y \rightarrow X}(\mathbf{x}, \mathbf{y}).$$

Proposition 1. Let $Z_1, \dots, Z_n \stackrel{iid}{\sim} \mathcal{N}(\mu, \sigma^2)$. Further define the standardized random variables

$$\tilde{Z}_i = \frac{Z_i - \bar{Z}_n}{S_n},$$

where

$$\bar{Z}_n = \frac{1}{n} \sum_{i=1}^n Z_i \quad \text{and} \quad S_n = \sqrt{\frac{1}{n-1} \sum_{i=1}^n (Z_i - \bar{Z}_n)^2}.$$

Then, for $i = 1, \dots, n$,

$$\tilde{Z}_i \xrightarrow{\text{a.s.}} \frac{Z_i - \mu}{\sigma} \sim \mathcal{N}(0, 1).$$

Proof

It is a well-known result in asymptotic theory that $\bar{Z}_n \xrightarrow{\text{a.s.}} \mu$ and $S_n \xrightarrow{\text{a.s.}} \sigma$. Thus,

$$(Z_i, \bar{Z}_n, S_n)^\top \xrightarrow{\text{a.s.}} (Z_i, \mu, \sigma)^\top$$

and applying the Continuous Mapping Theorem yields that

$$\tilde{Z}_i = \frac{Z_i - \bar{Z}_n}{S_n} \xrightarrow{\text{a.s.}} \frac{Z_i - \mu}{\sigma}.$$

From the property of normal distributions, it follows that $\frac{Z_i - \mu}{\sigma} \sim \mathcal{N}(0, 1)$.

Identifiability in Location-Scale Noise Models

In the following, we restate the theorem on the identification of location-scale noise models of [Immer et al. \(2023\)](#) for completeness. The authors derive a partial differential equation (PDE), which is required to be zero for all non-identifiable cases. They argue that only pathological cases which solve this differential equation exist.

Theorem 1 ([Immer et al. \(2023\)](#)). Assume the data is such that a location-scale noise model can be fit in both directions, i.e.,

$$\begin{aligned} Y &= f(X) + g(X) N_Y, & X &\perp\!\!\!\perp N_Y \\ X &= h(Y) + k(Y) N_X, & Y &\perp\!\!\!\perp N_X. \end{aligned}$$

Let $\nu_1(\cdot)$ and $\nu_2(\cdot)$ be the twice differentiable log densities of Y and N_X respectively. For compact notation, define

$$\begin{aligned} \nu_{X|Y}(x|y) &= \log(p_{X|Y}(x|y)) \\ &= \log\left(p_{N_X}\left(\frac{x - h(y)}{k(y)}\right) / k(y)\right) \\ &= \nu_2\left(\frac{x - h(y)}{k(y)}\right) - \log(k(y)) \quad \text{and} \end{aligned}$$

$$G(x, y) = g(x) f'(x) + g'(x) [y - f(x)].$$

Assume that $f(\cdot)$, $g(\cdot)$, $h(\cdot)$, and $k(\cdot)$ are twice differentiable. Then, the data generating mechanism must fulfill the following PDE for all x, y with $G(x, y) \neq 0$.

$$\begin{aligned} 0 &= \nu_1''(y) + \frac{g'(x)}{G(x, y)} \nu_1'(y) + \frac{\partial^2}{\partial y^2} \nu_{X|Y}(x|y) + \\ &\frac{g(x)}{G(x, y)} \frac{\partial^2}{\partial y \partial x} \nu_{X|Y}(x|y) + \frac{g'(x)}{G(x, y)} \frac{\partial}{\partial y} \nu_{X|Y}(x|y). \end{aligned}$$

B Computational Experiments

Notes on Implementation and Experimental Setup

We performed all experimental runs of SKEWD on CPUs of type Intel Xeon E5-2640v4 and Intel Xeon E5-4640v4 utilizing less than 10 GB RAM. We used Python version 3.11.5 on a Linux operating system.

In the following, we state the hyperparameter configurations used within SKEWD throughout all of the experiments analyzed in Section 6. We set $q = 14$ and $p = 7$ for the B-splines assuming that the scale function g is less complex than the location function f . In the CMA-ES optimization, we always used an adaptive learning rate, a step size of 1, and a population size of 100. The optimizer was set to terminate after a maximum of 5000 iterations or when the parameters barely changed within 25 iterations, specifically if $\|\theta^{(k)} - \theta^{(k-25)}\|_2 < 10^{-6}$. We also specified bounds for certain parameters for stability: $\rho \in [-10, 5]^p$ and $\lambda \in [-25, 25]$. The restriction on λ has a negligible effect on the skewness range, as the maximum absolute skewness that can be modeled through this restriction equals 0.9887, which is only slightly smaller than the actual maximum of 0.9953.

In the Bayesian optimization, we optimized the penalized likelihood on $k = 8$ folds with respect to α, κ . We sampled 40 initial candidates with Latin Hypercube Sampling on the log-scale within the range $(\log(\alpha), \log(\kappa))^\top \in [-4, 4]^2$. Additional 20 candidate values were selected based on the expected improvement acquisition function. As starting values for the final heuristic estimation, we used the $k = 8$ parameter estimates for θ which were obtained from the training folds during Bayesian optimization associated with the best pair $(\alpha, \kappa)^\top$. Additionally, further random starting values could be used for more robustness with respect to initial values. For the ECM algorithm, we allowed for a maximum of 5000 iterations, except for Tübingen pair 69, where we limited the iterations to 500 due to the large size of the dataset.

Graphical Comparison: Normal and Skew-Normal Distribution

SKEWD-IT fits skew-normal LSNMs in both directions $X \rightarrow Y$ and $Y \rightarrow X$. Based on the residuals from each model, the causal direction is inferred by comparing the independence of the cause-noise pairs. The independence-test version of LOCI works similarly, but assumes normally distributed noise.

For both SKEWD and LOCI, Fig. 3 shows fits and estimated residuals in the causal direction $X \rightarrow Y$ (3a, left) and the anti-causal direction $Y \rightarrow X$ (3b, right) for an exemplary pair from the novel skew-noise LSs(1.750) dataset. In both subplots of Fig. 3, the skew-normal model is depicted right, while the normal model is depicted left. The upper rows display the estimated mean and confidence intervals, whereas the cause-residual pairs are depicted in the lower row. In the causal direction (a), the estimated residuals in the normal-model show a dependence with cause X , indicated by the pointy outer contour level of the kernel density estimate (KDE) for small X , which is not present in the skew-normal model. In the normal-model, this dependence is incorrectly assessed as stronger by the HSIC test than the dependence exhibited in the anti-causal direction, seen in Fig. 3b. The skew-normal model, which is a generalization of the normal model, overcomes the shortcoming on this data pair by modeling the skewness, leading to seemingly independent residuals (oval KDE contour levels) in the causal direction compared to the anti-causal direction. Ultimately, LOCI infers the wrong direction, whereas SKEWD infers the true causal direction.

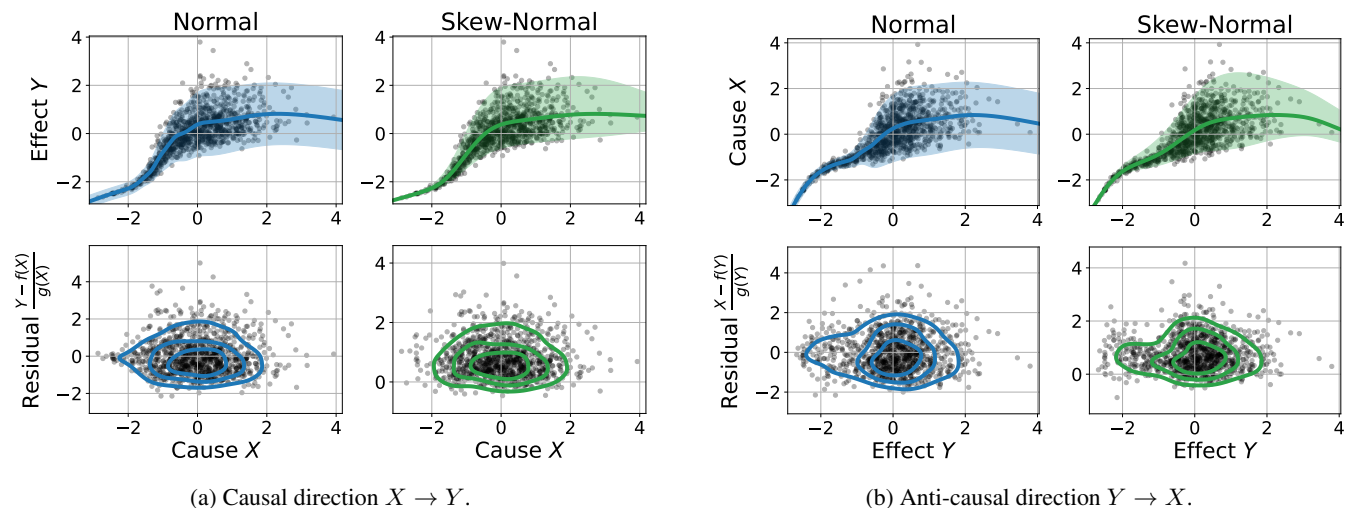


Figure 3: Comparison of LSNM mean fits, confidence intervals and residuals based on the normal distribution via LOCI (left in both (a) and (b)) and skew-normal distribution via SKEWD (right in both (a) and (b)) for pair 6 from the novel LSs(1.750) dataset.

Ablation of the ECM Algorithm

In Tab. 2, we show the accuracies on the novel skew-noise datasets for SKEWD-LL and SKEWD-IT as well as the accuracies that would have been achieved, if the heuristic parameter estimates via the CMA-ES in both directions were used to infer the causal directions. We denote the corresponding cause-effect methods as CMA-ES-LL and CMA-ES-LL. In the ANs case, the performance of the heuristic solutions is perfect in terms of likelihood scoring. However, when using independence testing, the refinement via ECM-algorithm in SKEWD leads to an increase in accuracy of 5% and 8.5% on the ANs(-0.455) and ANs(0.985) dataset, respectively. On the ANs(1.750) dataset, both independence-test versions achieve perfect accuracy.

The improvements in the performance on the causal task through the ECM algorithm in the LSs case are more critical. In that case, also the performance when using likelihood scoring is improved upon. Most notably by 12.5% on the LSs(0.985) dataset. The improvements for independence-based inference are much larger, ranging between 28% and 34%, demonstrating the necessity of refining the heuristic solution. This is further implied by the results in terms of AUDRC depicted in Tab. 3. Since they are mostly the same as in terms of accuracy, we do not further discuss them.

Method	ANs(-0.455)	ANs(0.985)	ANs(1.750)	LSs(-0.455)	LSs(0.985)	LSs(1.750)
SKEWD-LL	100.0	100.0	100	100.0	100.0	100
CMA-ES-LL	100.0	100.0	100	99.5	87.5	100
SKEWD-IT	98.5	97.5	100	86.0	82.5	92
CMA-ES-IT	93.5	89.0	100	52.0	54.5	64

Table 2: Accuracy in % over skew-noise datasets for SKEWD compared to the results if log-likelihood scoring and independence testing was performed based on the output of the CMA-ES-based heuristic. We denote these two versions of the heuristic as CMA-ES-LL and CMA-ES-IT.

Method	ANs(-0.455)	ANs(0.985)	ANs(1.750)	LSs(-0.455)	LSs(0.985)	LSs(1.750)
SKEWD-LL	100.00	100.00	100	100.00	100.00	100.00
CMA-ES-LL	100.00	100.00	100	99.99	93.68	100.00
SKEWD-IT	99.96	99.30	100	96.70	78.72	96.70
CMA-ES-IT	86.08	82.41	100	26.18	28.22	42.09

Table 3: AUDRC in % over skew-noise datasets for SKEWD compared to the results if log-likelihood scoring and independence testing was performed based on the output of the CMA-ES-based heuristic. We denote these two versions of the heuristic as CMA-ES-LL and CMA-ES-IT.

Tabulated Experimental Results

In this section, we present the exact results achieved by all baselines on the novel skew-noise datasets used in the experiments from Section 6. Tab. 4 reports the accuracy (in %) and Tab. 5 shows the AUDRC (in %) on the skew-noise datasets.

The results with respect to the established benchmarks are presented in Tab. 6 showing the accuracy (in %) and Tab. 7 showing the AUDRC (in %). Moreover, we report the mean accuracy and AUDRC (both in %) reached by all baselines across all 19 considered datasets in Tab. 8.

Method	ANs(-0.455)	ANs(0.985)	ANs(1.750)	LSs(-0.455)	LSs(0.985)	LSs(1.750)
SKEWD-LL	100.0	100.0	100	100.0	100.0	100
SKEWD-IT	98.5	97.5	100	86.0	82.5	92
LOCI-LL	100.0	99.5	83	100.0	96.0	66
LOCI-IT	99.5	99.5	98	72.0	69.0	75
ROCHE	99.5	97.5	95	99.5	88.5	81
QCCD	56.0	43.5	41	95.5	21.5	11
GRCI	87.5	80.5	93	79.5	69.5	84
CAM	100.0	100.0	100	82.5	70.0	33
RESIT	100.0	100.0	100	19.0	43.0	34
IGCI	38.0	38.5	56	30.5	53.5	88
IGCI-G	100.0	100.0	100	100.0	99.5	100

Table 4: Accuracy in % over skew-noise datasets.

Method	ANs(-0.455)	ANs(0.985)	ANs(1.750)	LSs(-0.455)	LSs(0.985)	LSs(1.750)
SKewD-LL	100.00	100.00	100.00	100.00	100.00	100.00
SKewD-IT	99.96	99.30	100.00	96.70	78.72	96.70
LOCI-LL	100.00	100.00	96.06	100.00	99.69	85.34
LOCI-IT	99.99	99.99	99.89	87.28	56.98	91.39
ROCHE	100.00	99.96	99.85	100.00	99.28	97.97
QCCD	57.15	26.68	27.93	99.68	0.62	1.41
GRCI	82.86	75.00	98.87	87.43	67.03	96.33
CAM	100.00	100.00	100.00	74.08	59.61	10.24
RESIT	100.00	100.00	100.00	47.79	70.50	43.61
IGCI	45.93	30.81	71.32	45.74	56.56	96.83
IGCI-G	100.00	100.00	100.00	100.00	99.99	100.00

Table 5: AUDRC in % over skew-noise datasets.

Method	AN	ANs	LS	LSs	MNU	SIM	SIMc	SIMln	SIMG	Tue	Cha	Net	Multi
SKewD-LL	100	100	100	100	87	54	51	81	88	45.97	54.33	73.33	72.00
SKewD-IT	100	100	87	97	88	78	82	86	81	66.57	77.00	84.33	78.33
LOCI-LL	100	100	100	100	100	49	50	80	78	53.00	43.00	77.00	72.00
LOCI-IT	100	100	94	89	100	78	82	73	78	60.84	72.67	86.67	79.00
ROCHE	100	100	100	100	100	78	82	77	81	77.27	74.00	87.67	83.00
QCCD	100	82	100	96	99	62	72	80	64	77.09	53.67	80.33	50.67
GRCI	100	94	98	87	88	77	77	77	70	81.59	70.00	84.67	77.33
CAM	100	100	100	53	86	57	60	87	81	57.77	46.67	78.33	34.67
RESIT	100	100	60	3	5	78	82	87	77	62.03	34.33	78.33	37.33
IGCI	20	35	46	34	11	37	45	51	53	68.03	55.00	55.33	92.33
IGCI-G	100	100	98	99	100	38	39	59	83	56.34	58.00	59.67	68.00

Table 6: Accuracy in % over established benchmark datasets. The Tübingen benchmark is abbreviated by Tue.

Method	AN	ANs	LS	LSs	MNU	SIM	SIMc	SIMln	SIMG	Tue	Cha	Net	Multi
SKewD-LL	100.00	100.00	100.00	100.00	97.58	64.58	64.33	94.57	94.95	54.57	57.50	81.93	92.01
SKewD-IT	100.00	100.00	93.71	98.62	97.78	90.36	93.83	96.78	93.67	69.71	77.47	96.30	83.21
LOCI-LL	100.00	100.00	100.00	100.00	100.00	59.94	63.74	94.73	88.95	67.02	47.25	86.17	92.66
LOCI-IT	100.00	100.00	99.41	97.42	100.00	88.74	93.16	85.97	93.24	59.62	71.33	96.97	77.76
ROCHE	100.00	100.00	100.00	100.00	100.00	86.61	93.85	88.96	92.43	75.46	78.42	97.62	94.40
QCCD	100.00	91.23	100.00	99.87	99.99	70.69	83.31	92.19	76.30	84.38	60.52	93.89	62.68
GRCI	100.00	99.62	99.67	95.14	97.18	89.62	92.38	92.09	87.69	73.23	70.81	95.97	73.60
CAM	100.00	100.00	100.00	36.29	76.45	67.76	68.82	87.20	88.24	69.37	41.05	84.88	40.02
RESIT	100.00	100.00	70.62	2.96	0.49	75.23	84.43	82.93	68.43	78.72	48.12	81.45	67.92
IGCI	17.83	35.45	59.54	48.98	1.27	34.49	40.86	51.34	62.88	73.81	58.39	61.23	98.75
IGCI-G	100.00	100.00	99.94	99.99	100.00	35.47	34.04	70.15	94.97	68.84	55.86	58.44	86.07

Table 7: AUDRC in % over established benchmark datasets. The Tübingen benchmark is abbreviated by Tue.

Method	Accuracy (%) \uparrow	AUDRC (%) \uparrow
SKEWD-LL	84.56 \pm 19.95	89.58 \pm 16.30
SKEWD-IT	87.46 \pm 9.53	92.78 \pm 8.92
LOCI-LL	81.39 \pm 20.60	88.50 \pm 16.51
LOCI-IT	84.54 \pm 12.71	89.43 \pm 13.63
ROCHE	89.52 \pm 9.92	94.99 \pm 7.56
QCCD	67.64 \pm 26.44	69.92 \pm 33.23
GRCI	82.93 \pm 9.07	88.13 \pm 11.05
CAM	75.10 \pm 23.17	73.90 \pm 26.44
RESIT	63.16 \pm 33.39	69.64 \pm 29.92
IGCI	47.75 \pm 20.20	52.21 \pm 23.97
IGCI-G	81.97 \pm 23.20	84.41 \pm 23.16

Table 8: Mean and standard deviation of accuracy, AUDRC over all 19 benchmarks. The top two approaches are bolded.

C Skew-Noise Datasets

In this section, we display scatter plots of 4 randomly chosen exemplary pairs per novel skew-noise dataset. We refer to Fig. 4 for ANs(-0.455), to Fig. 4 for ANs(0.985), to Fig. 6 for ANs(1.750), to Fig. 7 for LSs(-0.455), to Fig. 8 for LSs(0.985), and to Fig. 9 for LSs(1.750).

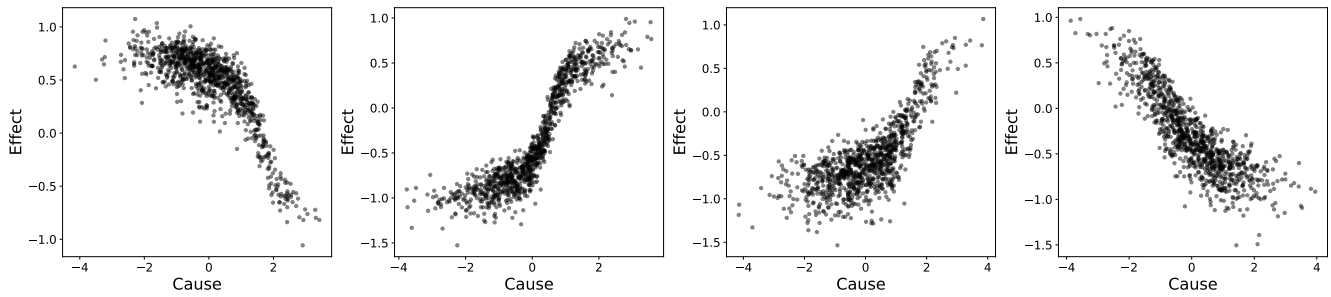


Figure 4: Exemplary pairs from the ANs(-0.455) dataset. Left two pairs generated with skew-normal noise, right two pairs generated with GNO noise.

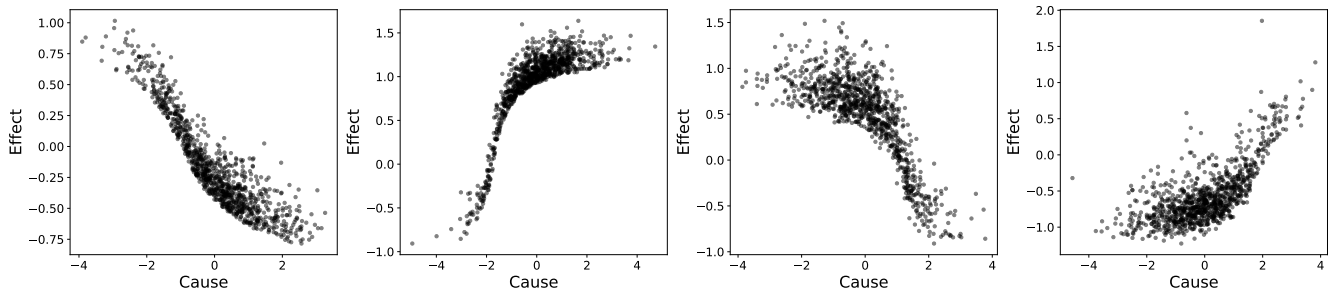


Figure 5: Exemplary pairs from the ANs(0.985) dataset. Left two pairs generated with skew-normal noise, right two pairs generated with GNO noise.

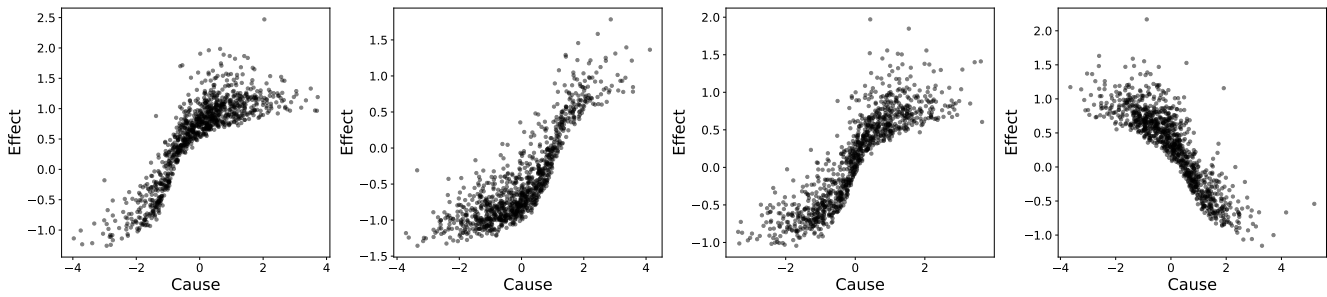


Figure 6: Exemplary pairs from the ANs(1.750) dataset.

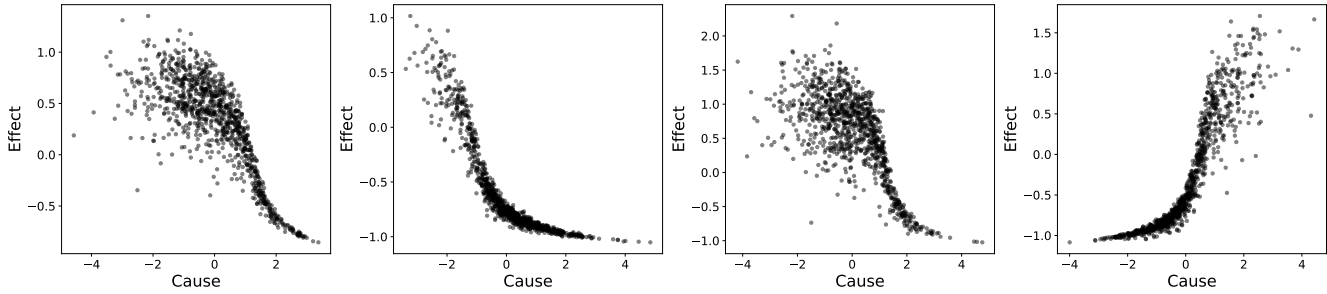


Figure 7: Exemplary pairs from the LSs(-0.455) dataset. Left two pairs generated with skew-normal noise, right two pairs generated with GNO noise.

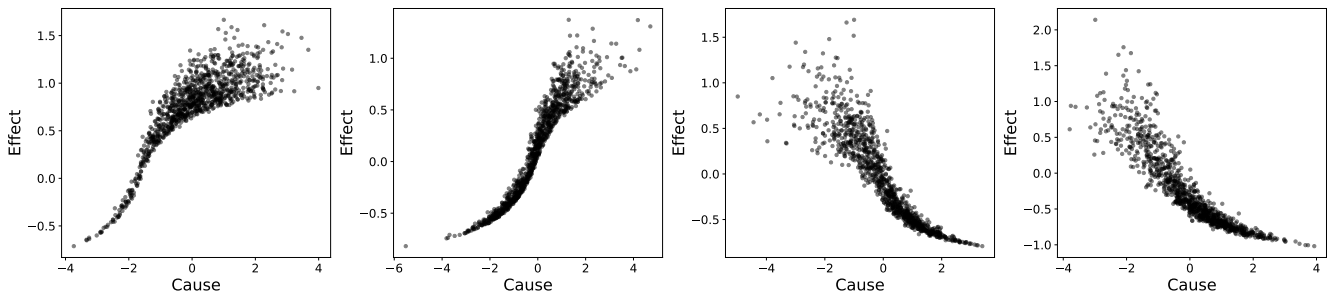


Figure 8: Exemplary pairs from the LSs(0.985) dataset. Left two pairs generated with skew-normal noise, right two pairs generated with GNO noise.

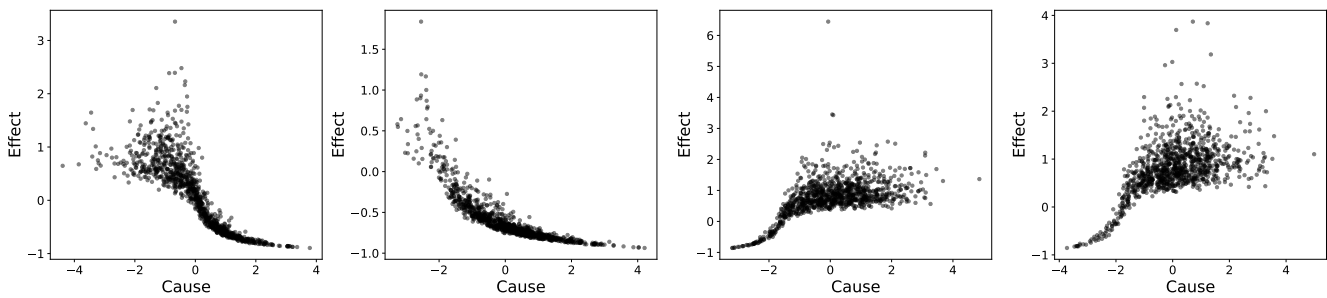


Figure 9: Exemplary pairs from the LSs(1.750) dataset.